

Design and Implementation of a 20 kW, 12000 RPM Permanent Magnet Synchronous Motor (PMSM) for the IST Formula Student Powertrain

João Viseu Sarrico

Formula Student is a worldwide competition for engineering students that gathers teams from universities all around the world with a common goal of design, manufacture and race with single-seat prototype cars. In the past, the Formula Student Técnico Lisboa Team - FST Lisboa - of the University of Lisbon has participated with seven cars, the last four being electric propelled vehicles, which are becoming more common on the track. All the previous four developed cars needed to be adapted to the available electric motor as these were directly acquainted in the market. This work provides the designing, manufacturing and testing of a tailored-made electric motor fully adapted for the race-car specifications. This choice made possible the improvement of the system, as the knowledge and the manufacturing of the electric motor could be fully “in-house” optimized, avoiding the dependency of the commercial solutions available in the market.

Index Terms—Formula Student Electric; Electric Race-car; Permanent Magnet Synchronous Motor; High Performance; Optimized geometry; Electric motor design; manufacture and test.

I. INTRODUCTION

THE electric motors have never been designed in the previous four Formula Student (FS) electric prototypes - Figure 1. In fact, over the past years, the electric motors that were used in the cars were always different. This happened as a result of the main philosophies, which changed from one car to the other, according to the results achieved and derived by the objectives established by the different teams. All the different powertrains used different commercial motors available on the market and, all the cars needed to be adapted in some way to the motors selected.



Fig. 1. FST 06e prototype car racing at Czech Republic.

In this research work, the requirements of the electric motor to be manufactured were decided taking into account the characteristics of some of the racing circuits of the FS competitions. In these competitions, the cars need to have very high lateral and longitudinal accelerations, as the overall tracks of those racing circuits have short straight lines and many corners. To achieve those accelerations, the weight of the car is a crucial parameter. Also beneficial is the use of one electric motor in each wheel, which allows the independent

control of each motor and thus increasing the car traction and overall performance. Other parameters must be taken into consideration whenever designing the motor, namely the very demanding regulation of the competitions, that limits some parameters. For example, the maximum power of the car is limited to 80 kW.

The first designing criteria adopted for the developed electric motor was that it would be fixed in the wheels suspension system, thus restricting its volume and weight. The voltage and current values supplying the motors would be imposed by the inverters made available by the team. Table I summarizes the goal parameters of the motors, taking into account the track steady state simulation carried out with the ideal car driven by the perfect driver - Figure 2.

TABLE I
MOTOR PROTOTYPE REQUIREMENTS.

Requirement	Value
Nominal Power	20 kW
Maximum Torque	20 Nm
Maximum Speed	12 000 RPM
Maximum Voltage	380V AC
Peak Current	100A
Cooling	Water

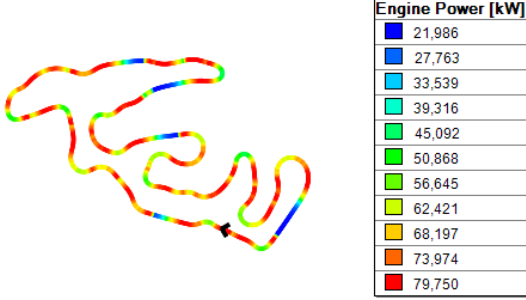


Fig. 2. Formula Student track power simulation.

II. SPOKE MACHINE MODEL

Brushless permanent magnets are currently the most commonly used electric motors for high performance electric race-cars, as they have higher torque/weight and power/weight ratio. They also have lower electrical and mechanical motor constants and are normally more electric efficient. However, these types of motors are expensive due to the high cost of the permanent magnets and are more sensitive to high temperatures, since the magnets can be partially or fully demagnetized, leading to a decrease in the motor lifetime [1] [2].

There are currently many topologies when analysing concentrate flux permanent magnets machines. The general advantage of these solutions is the possibility to concentrate the magnetic flux generated by the permanent magnets (PM) in the rotor and thus achieving higher air-gap flux densities. Consequently, these machines also have higher flux density in the stator windings. With this concentrating technique the PM requires lower values of magnetization, thus being protected against demagnetization and mechanical stresses [3].

A. Geometry

In this paper, the chosen magnetic circuit geometry was a *spoke* type, and it was developed in order to increase the air-gap flux density by the flux concentration principle. It promotes the flux concentration, as the sum of magnets surface areas is greater than the rotor surface area. Furthermore, it has the benefit of using typical rectangular PM blocks, reducing their costs. One of the limitations of this geometry is the material required for the shaft, i.e., a non-ferromagnetic material is necessary or else a large portion of the flux generated by the PM would leak through it.

Figure 3 shows the *spoke* type rotor configuration used and its decision variables that will be further discuss in the next chapter.

B. Windings Layout

An algorithm was used independently to optimize the windings layout [4]. The algorithm distributes spatially, per slot, the windings phases to maximize the fundamental magnetomotive force (mmf) harmonic per ampere while minimizing the resultant induced current stator (mmf) harmonics and maximizing

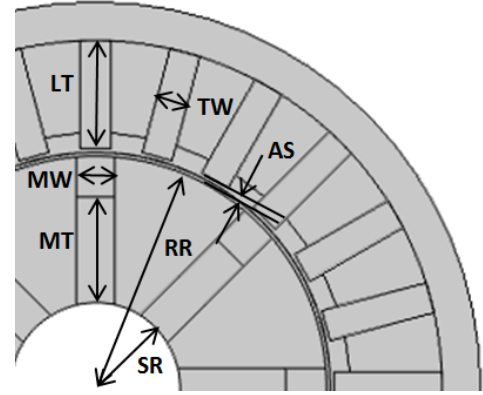


Fig. 3. Cross-section of *spoke* geometry with the geometric parameters.

the balanced windings conditions by defining a proper winding arrangement.

The higher the number of slots within one rotor pole per phase, the more sinusoidal the final magnetomotive force, and consequently, the motor will present a lower torque ripple and higher efficiency since it will have low harmonics content. However, a proportional relation between the number of slots per pole per phase and the fundamental winding factor does not exist. This happens because when the winding assigned to each phase is distributed by the stator slots, the Electromotive Force (EMF) induced on the different slots is not in phase and their sum will be less than the numerical sum. Therefore, the winding factor should be the highest possible to maximize the EMF induced at each phase [4].

The fundamental winding factor is maximum for three poles/slots combination taking into account that:

- The number of coils of each phase must be multiple of the number of phases;
- The number of coils of each phase is equal to the number of slots.

Simulations were carried out to determinate the best configuration for this case. The results are shown in Table II where the fundamental mmf amplitude per amp, sum of the harmonics per amp and balanced condition were analysed.

TABLE II
DIFFERENT WINDINGS LAYOUT CHARACTERISTICS.

Study	Fundamental	Sum Harmonics	Balanced
12 slots / 6 poles	0.574	1.79	Yes
12 slots / 8 poles	0.414	1.169	Yes
12 slots / 10 poles	0.369	2.137	No
24 slots / 6 poles	0.979	2.512	Yes
24 slots / 8 poles	0.956	0.414	Yes
24 slots / 10 poles	0.732	2.394	Yes
30 slots / 6 poles	1.501	2.630	No
30 slots / 8 poles	1.12	3.576	No
30 slots / 10 poles	0.902	2.097	No

Single layer coils were selected, aiming at manufacturing process of the prototype as less complex as possible. In fact, at this stage, the objective was to build a motor prototype to

validate the theoretical simulations. With that aim, it is possible to reduce errors associated with the motor's construction.

Taking the previous into account, the number of slots that maximize the fundamental winding factor was found to be 30 (with 6 poles), once it has the highest fundamental mmf per amp. However, it has high sum of harmonics, which will increase the heat production and do not have a balanced condition. Winding with 24 slots and 8 poles with 0.956 fundamental mmf per amp, 0.414 sum of harmonics and balanced condition was the selected one, as it has the best commitment between the fundamental mmf and harmonic losses and also has balanced condition. The adopted winding configuration is shown in Figure 4.

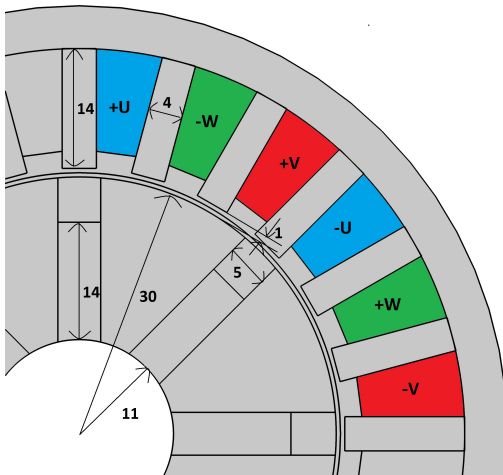


Fig. 4. Winding configuration of the optimized geometry.

III. DESIGN OPTIMIZATION

Electromagnetic, thermal and mechanical phenomena are strongly interdependent by non-linear relations. A modification in one dimension can lead to changes on the specifications of the motor. Nowadays, with the increasing of the computational resources and with the development of finite element analysis tools (FEA), it is possible to calculate with enough accuracy the power, torque, losses and other motor's performances.

The optimization algorithm used to assist the motor design in this research was a single objective genetic algorithm (GA). The optimization process is shown in Figure 5, where the genetic algorithm works together with a FEA software to produce the optimum solutions, under a set of constraints. The maximum torque value obtained is returned to the optimization algorithm and a score is defined based on the constraints and torque results. The best results of each generation move to the next iteration, depending on the user definitions (elite count). For the optimized machine design solution, the mechanical and thermal models are analysed iteratively [5].

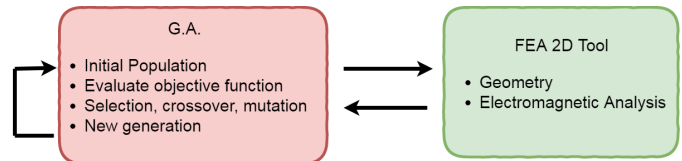


Fig. 5. Optimization process carried out.

1) Objective Function

The objective function of the algorithm consists in minimizing the negative value of the maximum motor torque (Equation 1). It is considered that the maximum torque will be produced at the maximum feeding current available from the inverter, without saturating the magnetic core.

$$\min_{x \in \Omega} F(x) \equiv (-f_1(x)) \quad (1)$$

2) Decision Variables

The motor geometry is created according to the seven decision variables presented in Table III. These variables are integers with a step of 1 mm because it is not expected to adopt very high manufacturing tolerances. It also decreases the entire population space in order to converge more rapidly.

TABLE III
MOTOR DECISION VARIABLES

Design Parameter	Variable	Range
Rotor radius	RR	20-40 mm
Magnet width	MW	1-7 mm
Magnet length	ML	5-15 mm
Teeth width	TW	1-10
Teeth length	TL	7-20 mm
Air-gap size	AS	1-5 mm
Shaft radius	SR	5-30 mm

These decision variables define the 2D geometry of the motor; a representation is shown in Figure 3.

3) Constraints

Table IV presents the constraints values that physically limit the motor manufacturing. Some others constraints must also be considered, for instance, the weight and the magnetic flux density which must also be limited. The first limit is imposed by the user according to the requirements and the second one is defined by the magnetic saturation value in the magnetic core materials. Therefore, the material chosen for the magnetic material is NO20.

TABLE IV
MOTOR DECISION VARIABLES

	Design Constraint	Constraint
Geometrical	Weight	<5Kg
	Stator outer radius	50 mm
	Stack lenght of the motor	80mm
Inverter	Maximum motor current - peak	50 A
	Copper winding temperature	180°C
Thermal	Permanent magnet temperature	120°C
	Magnetic flux density	<1.9T

IV. OPTIMIZATION RESULTS

More than 50 studies were made, with a total computing time of 1135 hours. These were divided into 4 categories: the “preliminary tests” (where the algorithm was tuned to work without errors) and the “12 slots”, “24 slots” and “30 slots” according to the number of slots of the motor Table V. Inside each category, geometries vary between 4 to 10 magnetic poles were also analysed.

TABLE V
NUMBER OF POPULATION ELEMENTS AND GENERATIONS

Category	Number of Studies	Time of Studies [h]
Preliminary tests	24	181
12 slots	16	429
24 slots	5	170
30 slots	8	355
Total	53	1135

The best optimization results are shown in Table VI, being in this document only analysed the best torque values results.

TABLE VI
ALGORITHM RESULTS

Category	Torque [Nm]	Weight [Kg]
12 slots	15.27	5.0
24 slots	25.50	4.49
30 slots	14.47	4.86

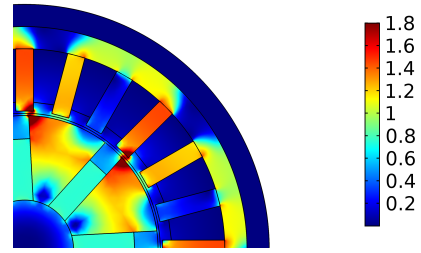
The optimized values of the algorithm are presented in Table VII.

TABLE VII
MOTOR OPTIMIZATION RESULTS

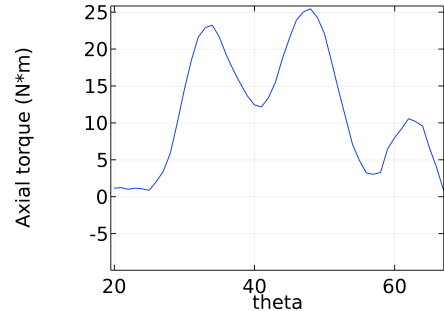
Design Parameter	Variable	Optimized
Rotor radius	RR	30 mm
Magnet width	MW	5 mm
Magnet length	ML	14 mm
Teeth width	TW	4 mm
Teeth length	TL	14 mm
Air-gap size	AS	1 mm
Shaft radius	SR	11 mm

The geometry with 24 slots was selected as it presented the highest torque value. Due to the high FEA simulation times, the population size and number of generations were set to 10 and 50, respectively. For those a time of approximately 45 to 50 hours were required to perform the optimization. Further analyses were conducted to the magnetic flux density and torque value along time, namely for a sinusoidal current wave feeding the motor terminals, as shown in Figure 6.

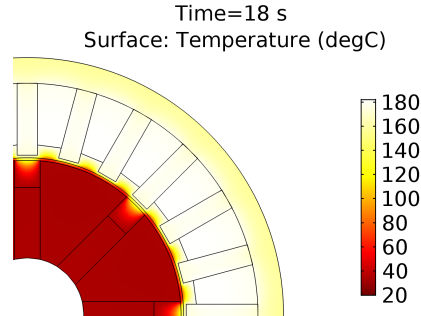
Surface: Magnetic flux density norm (T)



(a) 2D magnetic flux density of the result with 24 slots.



(b) Simulated prototype torque.



(c) Thermal Simulaton 2D.

Fig. 6. FEA Result for the best geometry.

It is possible to conclude that the maximum torque is about 26 Nm at an angle of the rotor (theta) of 51 degrees, at this value there is not magnetic saturation in the core, as the maximum registered value is 1.8 T. This result is higher than the defined value as the objective which gives a margin to the iterations of the mechanical and thermal model to be implemented in order to improve the motor robustness and allow its manufacture. The thermal studies showed that the MJF motor can withstand up to 18 seconds the peak torque, considering an initial temperature of 30°C, without a cooling system. After 18 seconds the windings will reach their maximum temperature (180°C), and since this is a short period of time, the rotor PM will not reach temperatures over 37°C.

V. PROTOTYPE DESIGN

After the best result of the optimization, some modifications were made to the magnetic circuit to be possible to manufacture the machine's prototype. First, fins were added to the shaft in order to hold the rotor pieces in place. Those fins must withstand the centrifugal forces of the rotor spinning at 20 000 RPM. To resist such high forces, the angle towards the radius was increased in order to prevent the rotor piece from slipping, Figure 7. After that, to facilitate the rotor manufacturing, the different pieces were joined resulting in one part only. With this configuration, only one mould is required and the manufacturing costs can be reduced.

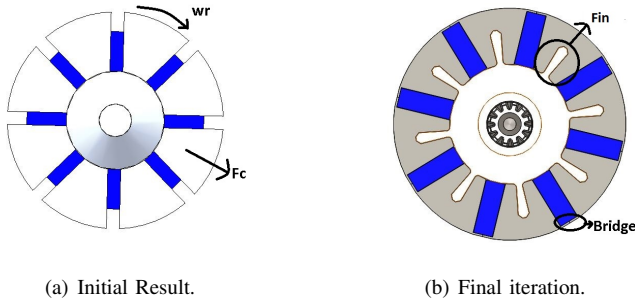


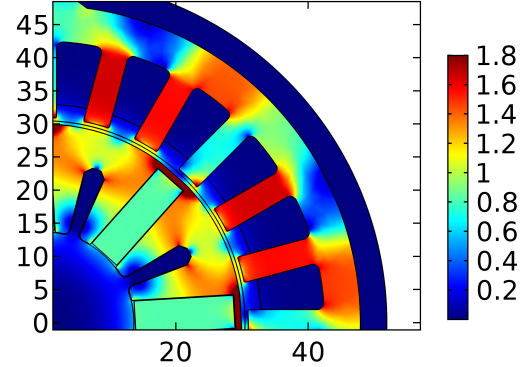
Fig. 7. Rotor geometry.

A. Electromagnetic model

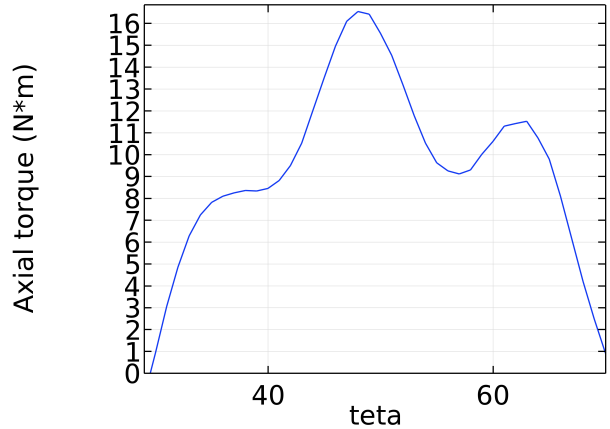
The magnet-bridges added (which also help the magnets withstanding the centrifugal forces) become saturated as high magnetic fluxes pass by. This decreases the flux in the air-gap, decreasing the torque per ampere production and the torque of the motor. However, it increases the losses.

From Figure 8 it is possible to conclude that these iterations lead to a 20% decrease of the motor maximum torque from 25.5 to 20.7. This effect is mainly due to the existence of the rotor bridges in the top of the magnets which decrease the magnetic flux between the rotor and the stator, decreasing the torque production. Moreover, the shaft diameter was increased in order to withstand the rotor forces. Additionally, the material used in this simulation (NO20) is different from the material used in the optimization algorithm (Standard magnetic iron). Nevertheless, this value was considered to be sufficient to continue with the manufacturing of the motor, as it was considered that this torque percentage decrease would be about the same value in the others optimization results that had initially less torque. It is also important to notice that this geometry is capable of withstanding the temperatures generated at peak torque with a duration up to 16 seconds.

Surface: Magnetic flux density norm (T)

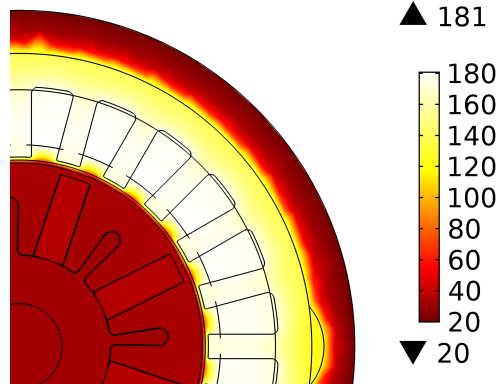


(a) 2D magnetic flux density of the final result with 24 slots.



(b) Simulated prototype torque.

Time=16 s Surface: Temperature (degC)



(c) Thermal Simulation 2D.

Fig. 8. FEA Result of the final version with 24 slots.

1) Tooth lips of the stator

The tooth lips of the stator were analysed too. They support the copper windings on the slots and prevent them from falling to the air-gap with the vibrations of the motor and the electromagnetic forces caused by the currents and magnetic flux density in the wire.

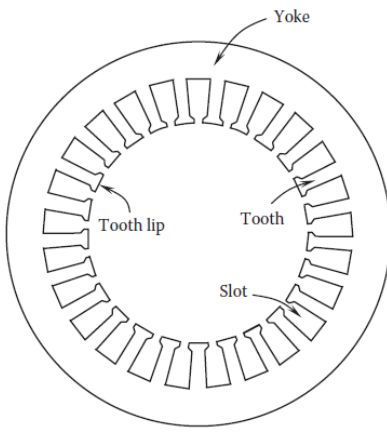


Fig. 9. Stator with tooth lips.

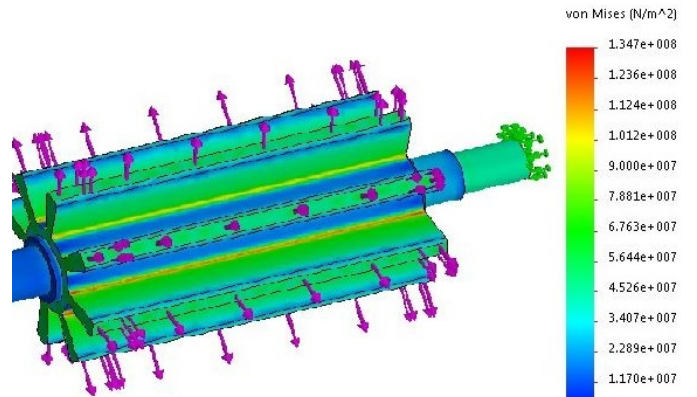
Simulations were made to the electromagnetic geometry considering two different cases: a stator without lips and a stator with lips. These simulations showed a decrease of about 15 % of the output torque. Although the ripple is expected to decrease considerably, the difference of torque in this motor when using lips in the stator slots is large enough to continue with the first solution (without lips). This solution will complicate the work of winding the motor and can raise problems as retaining the windings in the slots, preventing them from going to the air-gap. The solution founded to overcome this problem was to add a special coating of epoxy to fix the windings.

B. Mechanical model

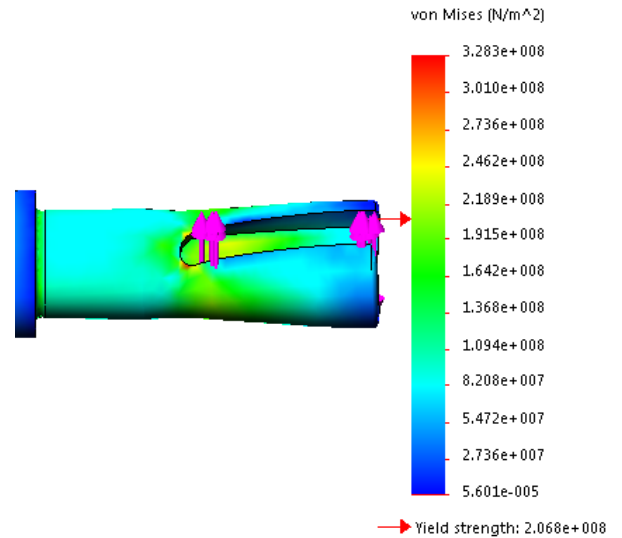
In a motor, the shaft must be capable of withstanding all the centrifugal forces of the rotor and is, therefore the component that is most severely subjected to the mechanical forces. In fact, considering that each spline hold one of the eight pieces of the rotor and one magnet, and that they rotate at 20 000 RPM the force that each spline is subjected to approximately 18000 N. The material selected for the shaft was AISI 316 Stainless steel materials, non-ferromagnetic material.

To begin with, the analysis of the shaft to assure that the motor could handle the centrifugal forces in case of overspeed, dictated some modifications on the rotor. Further analysis regarding the magnets mechanical behavior were also done. The stator practically did not changed during the process: the only alteration performed was regarding a key, that was added on the stator outer diameter to assure that it would not spin in relation to the motor housing. This was done because one of the motor requirements is to have the capacity of being totally disassembled: this requirement made impossible to assure the stator is constrained by applying the ideal mechanical tight fit.

Special attention was given to the following load cases:i) centrifugal force due to rotor rotation on the shaft fins; ii) the maximum torque generation.



(a) Simulation of the fins when rotating at 20 000RPM.



(b) 20Nm torque load on the key seat.

Fig. 10. FEA static nodal stress on AISI 316 Stainless Steel material.

Results in Figure 10(a) proved as expected, that the fins base is the most sensible area due to its short thickness. The simulation carried out previously showed the material can withstand the forces with a mechanical Factor of Safety (FoS) [6] of 2.15.

In Figure 10(b) it is possible to understand that the maximum stress produced is 328.3 MPa. Although it happens in a very specific and short area, where a chamfer exists, this together with the visualization of the stresses, that are considerably less in the surrounding area, suggest that it is a singularity. It was assumed that the shaft could hold the forces created when the motor is generating the maximum torque. Some displacement is expected, but as the value is within the ultimate tensile strength of 580 MPa, the material will not fail. A thermal treatment for the shaft material will be required to increase the value of its surface yield strength.

C. Thermal model

2D simulations were conducted under the scope of this work, to assure that the thermal limits of the motor are not reached when maximum power is provided (Figure 6(c)), where the initial temperature set on the simulation was 30 °C. The total losses of the motor in the peak power situation, with a torque of 20 Nm at 9500 RPM, are the following in the thermal simulation: i) 4500 W in the coils; ii) 80.6 W in the magnets, iii) 46.6 W in the rotor core; iv) 65.6 W in the stator yoke core; v) 76.6 W in the stator teeth core.

A more detailed analysis of the motor thermal behavior (Figure 11) and of the cooling system design and study (Figure 12) were done in 3D, under the scope of another FST Lisboa team member, who was responsible for the car cooling system - Pedro Fontes [7]. Those simulations were conducted taking into account the nominal torque (and power) instead of the peak values, as the cooling system is designed to assure that the motor does not overheat during one endurance race using the average power that the car needs.

The geometry of the cooling jacket of the motor was optimized so that the maximum temperature of the magnets would not exceed 120°C. The initial temperature of the water was set at 30°C and the total power losses were considered as follows: i) 2200 W in the windings by Joules Losses; 20.6 W in the rotor; 61.5 W in the stator by iron losses. These values correspond to the losses at the nominal power of the motor.

Figure 11 shows that the maximum simulated temperature in the magnets is 116.3°C which lays inside the defined requirements.

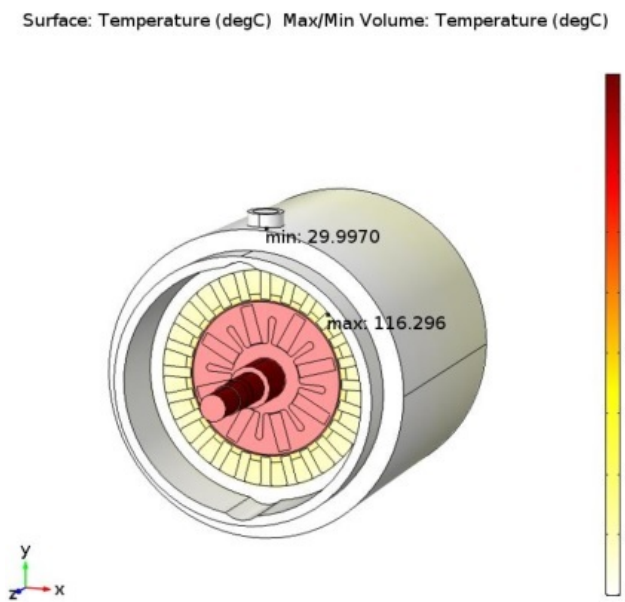


Fig. 11. Motor temperature with water cooling considering about 2300 W power losses.

Figure 12 shows the water temperature variation when dissipating about 2300W of power losses. This result is relevant as the cooling system of the car has other components in series that receive the water coming from the motors.

Surface: Temperature (degC) Max/Min Volume: Temperature (degC)

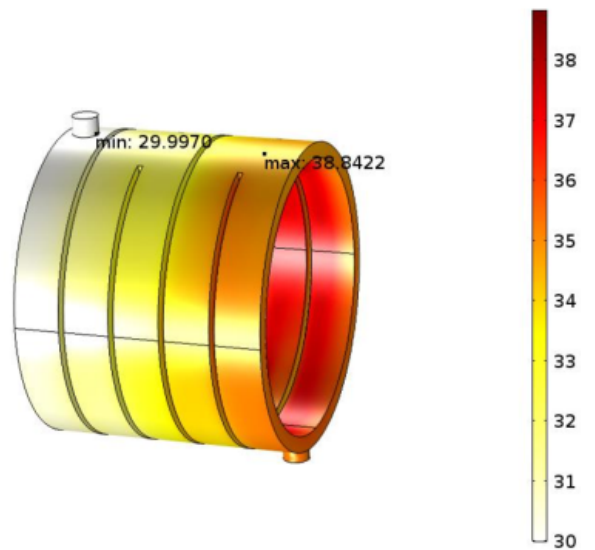


Fig. 12. Water temperature when it is dissipated 2300 W on the motor.

D. Number of turns per coil

After the winding configuration was selected and the motor geometry was set, the number of turns of each coil was analysed. The goal was to have a voltage constant (k_e) similar to the AMK motor - 18.8 V/kRPM to be used instead in case of a major failure. This BEMF was calculated according to Equation 2, where ϵ is the Electromotive force voltage [V], w is the mechanical frequency of the rotor [rad/s], pp is the number of pair of poles, N_T is the number of turns of each coil and $\bar{\phi}_{coil}$ is the flux of each coil [Wb] taken from FEA simulations ($\bar{\phi}_{coil} = 0.0016Wb$). The results obtained, considering the previous equation are shown in Equation 2 for 4, 10 and 20 turns per coil.

$$\epsilon = jw \times pp \times N_T \times \bar{\phi}_{coil} \quad (2)$$

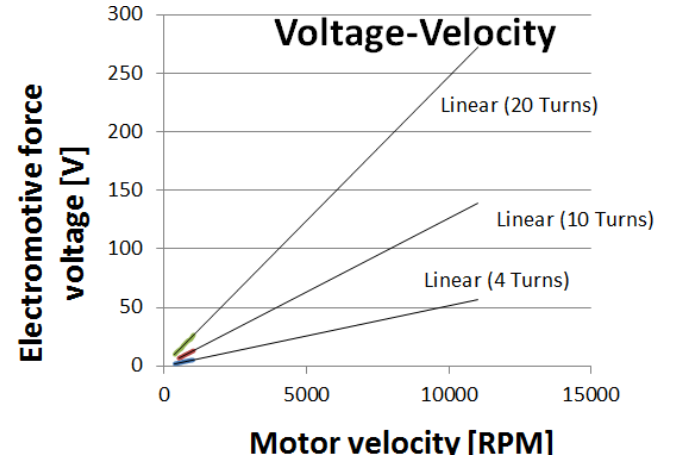


Fig. 13. Variation of the electromotive force voltage with the coils number of turns.

It is important to refer that this theoretical graph does not take into consideration possible non-linear phenomena as core flux saturation, nevertheless without load it would only happen at speeds higher than 12 000 RPM. The selected solution was to adopt coils with 20 turns, as this configuration (with a k_e of 22 V/kRPM) is closer to the k_e AMK value. Additionally, with 20 turns it is expected that the peak current to generate the maximum torque will be lower, as it decreases with the number of turns per coil.

E. Motor Efficiencies

Efficiencies were calculated using Equation 3, Equation 4, Equation 5 and Equation 6, where P_{total} refer to the total power losses of the motor [Watt], P_{Joule} the Joule losses P_{Iron} losses in the Iron by the Eddy phenomenon, K_{hyst} is the hysteresis constant of the material, B is the magnetic flux density [T], f the electric frequency [Hz] and K_{Eddy} the Eddy constant [8].

$$P_{total} = P_{Joule} + P_{Iron} \quad (3)$$

$$P_{Iron} = K_{hyst} B^2 f + K_{Eddy} \times (B f)^2 + K_{exc} (B \times f)^{1.5} \quad (4)$$

$$\begin{aligned} K_{hyst} &= 0,0166 \\ K_{Eddy} &= 1,174E - 5 \\ K_{exc} &= 6,112E - 4 \end{aligned} \quad (5)$$

$$\epsilon = \frac{P_{mechanic}}{P_{mechanic} + P_{total}} \quad (6)$$

Figure 14 was traced assuming values calculated considering a range of torque varying from 0 to 20 and the velocity varying from 0 to 12 kRPM.

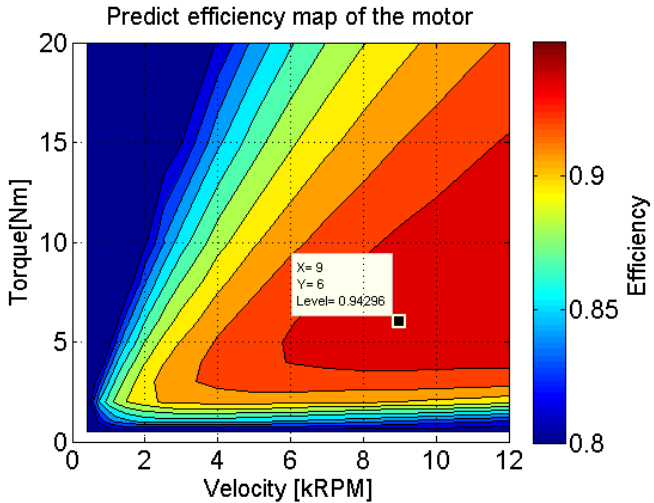


Fig. 14. Predicted efficiency map of the motor.



Fig. 15. Render of the MJF motor CAD.

F. CAD model

The final product of the motor prototype is presented as a computer-aided design (CAD), after all the different design phases: materials and topology selection, manufacturing methods, requirements definition, winding optimization, electromagnetic optimization, mechanical and thermal analysis (Figure 15). The CAD is a 3D picture of all the technical drawings and dimensions set for the motor, which means that, at this phase, it is possible to send all the pieces of the motor to be manufactured.

G. testbench

In order to conduct the tests for the velocity, torque, power, efficiency and endurance, a testbench was built (Figure 16). This testbench was composed by two electric machines, the MJF motor and a Siemens motor used as a generator mechanically attached by two transmission boxes (one 4:1 and other 1:20, which gives an final ratio of 1:5). The generator was connected to a rectifier that was connected to a load. The motor was connected to a battery through an inverter.

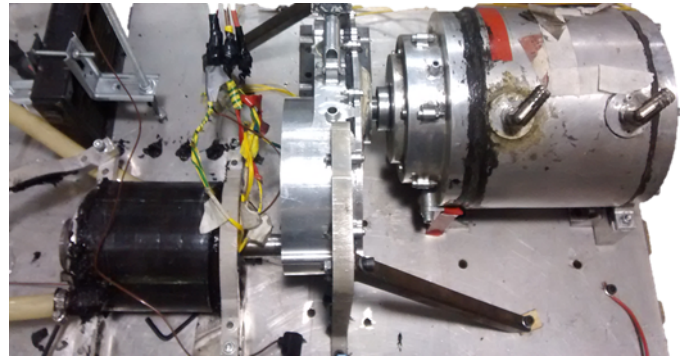


Fig. 16. Motor testbench.

VI. MOTOR TESTING

In this work, the most relevant tests to determine the defined motor parameters were: i) motor number of turns per coil, ii) maximum velocity, iii) maximum torque, iv) maximum power, v) nominal performance during endurance simulations and vi) efficiency.

The first test was done to validate the number of turns per coil that match the back electromotive force (BEMF) voltage imposed by the inverter without exceeding the maximum temperature of the motor. The second test was performed to observe if the rotor could withstand the centrifugal forces at maximum velocity and also to analyse if the voltage induced in the phases of the motor were coherent with the calculated BEMF voltage. To validate the torque, a third test was conducted; during this test the goal was to observe if the motor was capable of producing the design torque, without saturating the core and without exceeding the maximum current of the inverters. Knowing the maximum velocity and torque, the next test was carried out to validate the maximum power of the motor without exceeding the maximum temperature of 80°C. After, an endurance test at nominal performance was performed to validate the working range parameters of the motor during 25 minutes and to validate the behavior of the cooling system. At last, a test was made to determine the efficiency of the motor at different speed and torque points.

A. Efficiencies test

To determine the practical efficiency of the MJF motor, a watt-meter was connected to each motor phase to measure voltage and current waveforms. With these measurements, the instant power can be calculated. The output mechanical power was measured in the Siemens machine side, so this value also includes the efficiency of the two transmission boxes that decrease the final efficiency value of the MJF motor.

The efficiency of the two transmission boxes are not considered on this table, as their real values are not known. In fact, looking at their mechanical tests, it is possible to see that the first has a theoretical efficiency of about 98% and the second of 96%. The repetition of this test with a proper testbench, where the mechanical power is measured without the influence of a transmission box, is recommended to be performed in the future.

With all the pair of values recorded during the test and using a Matlab script, it is possible to draw the efficiency map presented in Figure 17. It can be concluded that the value of the maximum efficiency is high (around 94%), proving the characteristic of synchronous machines. The efficiency at low velocities and low torque are small due to constant losses predominance over the work done.

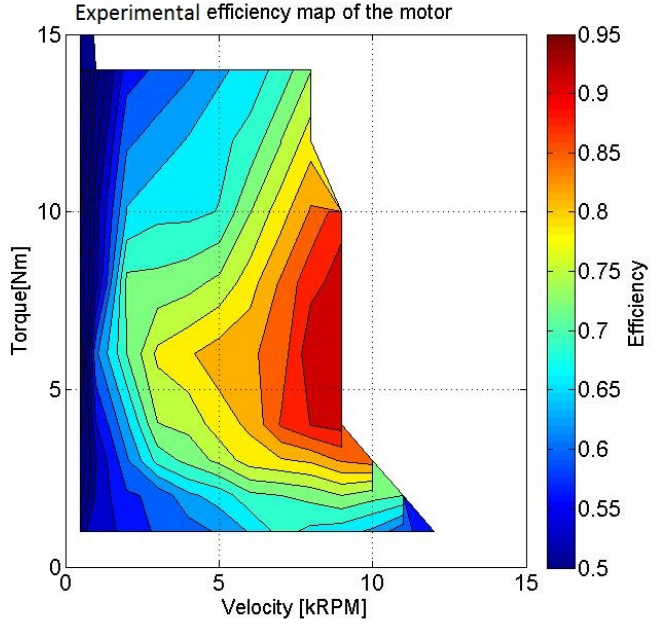


Fig. 17. MJF efficiency map tested.

B. Performance tests

From the torque-speed graph (Figure 18(a)) one can see, all the points taken during the different tests, and trace the equivalent graph (red). With these points is possible to trace the maximum torque-speed real curve of the MJF motor in case of no testbench limitations had occur (purple graph). To trace this graph it is assumed the maximum torque is maintained to the speed the BEMF voltage is equivalent to the maximum voltage the inverter is capable of feeding (6500 RPM). After that point, the torque decreases linearly to zero torque, when the motor reaches its maximum speed. Although, this was not tested, it is possible to estimate that graph, doing the two test separately (velocity with lower torques and torque with lower velocities). Green graph shows the torque-speed curve for the MJF motor with 10 turns per coil instead of 20. All the graphs are considering a battery voltage of 600 V.

The same happens with the power-speed curve (Figure 18(b)), because it was not possible to test all the working range points of the motor, mainly the ones having high torque at high rotor speeds, the real tested power was less than the expected one (the estimated curve of the maximum power without test limitation is represented on purple). On green is the power-speed curve for the MJF motor with 10 turns. One can conclude that the motor cannot perform more than 13.5 kW with a feeding battery voltage of 600 V. To the 20 kW, the battery should have around 700 V. Since it is not possible in Formula Student the solution passes by decreasing the number of turns per coils to 10, with no consequence to the maximum generating torque ability of the motor.

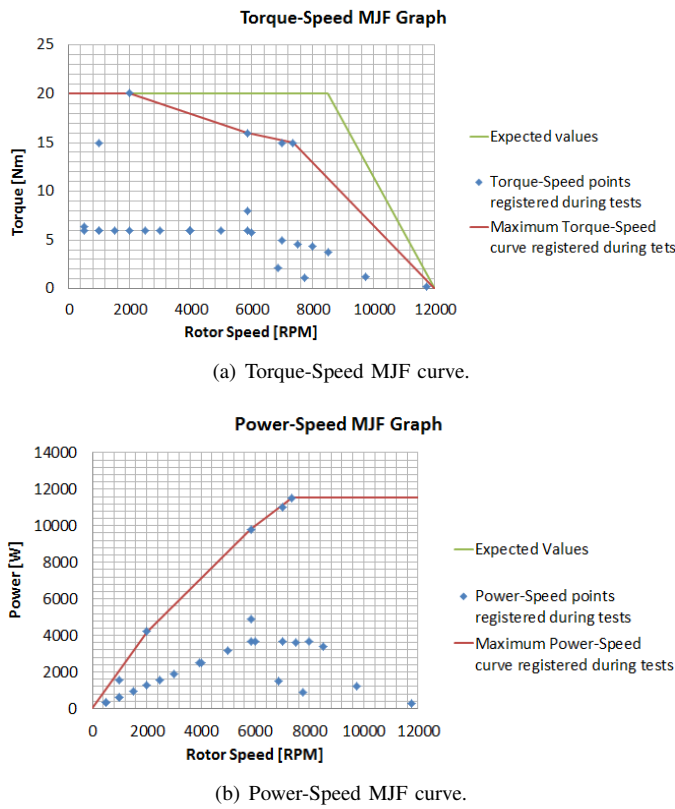


Fig. 18. Torque-Speed and Power-Speed MJF curves.

VII. CONCLUSION

In Figure 19 a comparison between theoretical and experimental results in performed, considering no limitations of the testbench had occurred. A decrease of the maximum torque (from 20.5 to 20 Nm) and the base speed (from 9 500 RPM to 8 500 RPM) was observed. The first one due to the expected manufacturing influence on the motor, and the second because the terminal induced voltage at 20 Nm @ 8 500 RPM was higher than the calculated. As a consequence, the peak power decreased from 20.5 kW to 18 kW.

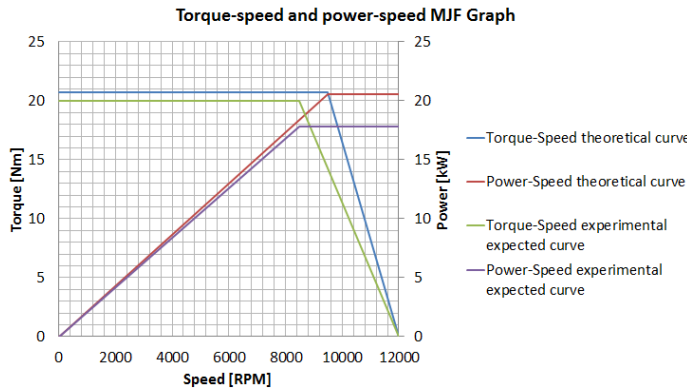


Fig. 19. MJF theoretical and experimental results.

Nevertheless, and with some minor modifications, the work carried out showed the possibility of design and manufacture a competitive tailored motor. With this, it is possible to design a geometry adaptable to a racing environment instead of

adapting a commercial solution which is more expensive and have more standards, some of them not important for the application.

The work carried out resulted in the manufacturing of the MJF electric motor prototype which will serve as testing and validation model for the future and improved versions to integrate the powertrain of the FST 08e car. The electric motor prototype developed proved, according to the tests carried out, to comply with the defined requirements defined by the FST Lisboa team.

REFERENCES

- [1] D. C. Hanselman, *Brushless permanent magnet motor design*. Magna Physics Publishing, 2006.
- [2] W. Tong, *Mechanical Design of Electric Motors*. CRC Press, 2014.
- [3] B. Ricardo da Fonseca Marques, "Virtual Prototyping of a Brushless Permanent Magnet AC Motor - Electromagnetic and Thermal Design using CAD Software," Master's thesis, Instituto Superior Técnico, 2012.
- [4] D. Delgado, "Automated AC winding design," Master's thesis, University of Manchester, 2009.
- [5] A. Santos, "Dynamic analysis and design of impact attenuator structures for a Formula Student prototype," Master's thesis, Intituto Superior Técnico.
- [6] J. K. N. R. G. Budynas, *Shigley's Mechanical Engineering Design, Ninth Edition*. New York: McGraw-Hill, 2011.
- [7] P. M. d. A. Fontes, "Refrigeração do propulsor elétrico de um veículo Formula Student," Master's thesis, Universidade de Lisboa, 2016.
- [8] L. Pinto, "Integrated Electrical Generators in Aircraft Turbines Thermal analysis of a front-low rotation 90 kVA PM synchronous auxiliary generator," Master's thesis, Instituto Superior Técnico, 2015.